Supporting Information

Studying the Polymerization Initiation Efficiency of Acetophenone-Type Initiators via PLP-ESI-MS and Femtosecond Spectroscopy

Elena Frick,[†#°] *Hanna A. Ernst,*[‡°] *Dominik Voll,*[†#] *Thomas J. A. Wolf,*[##] *Andreas-Neil Unterreiner,*[‡*] *Christopher Barner-Kowollik*[†#*]

[†]Preparative Macromolecular Chemistry, Institut für Technische Chemie und Polymerchemie, Karlsruhe Institute of Technology (KIT), Engesserstr. 18, 76131 Karlsruhe, Germany, christopher.barner-kowollik@kit.edu

[#]Institut für Biologische Grenzflächen, Karlsruhe Institute of Technology (KIT), Hermann-von-Helmholtz-Platz 1, 76344 Eggenstein-Leopoldshafen, Germany

[‡]Institut für Physikalische Chemie, Abteilung für Molekulare Physikalische Chemie, Karlsruhe Institute of Technology (KIT), Fritz-Haber-Weg 2, 76131 Karlsruhe, Germany, andreas.unterreiner@kit.edu

[##]Stanford PULSE Institute, SLAC National Accelerator Laboratory, Menlo Park, CA 94025, USA

[°]These authors contributed equally to this publication.

Trio PLP Experiment. A trio PLP experiment with all three initiators together in one sample in the molar ratio 1:1:1 was carried out in order to summarize the binary cocktail experiments with two photoinitiators, respectively (see **Figure S1**). The initiation ability of the benzoyl fragment of Bz clearly surpasses both MMMP fragments (T and N) as well as the 4MB fragment. At the same time, in contrast to the results of the experiments with two compared initiators, the T and MB fragments show almost equal initiation abilities. A possible explanation could be that competing ionization processes, based on the high number of different end group functionalities in the trio experiment, can have an influence on the ionization of particular polymer chains. Therefore, due to end group-biased ionization effects explained in the main text (see *Ionization and Solubility Effects in MMMP-initiated Polymer)*, a direct comparison (as depicted in **Figure S1**) is possibly inappropriate.

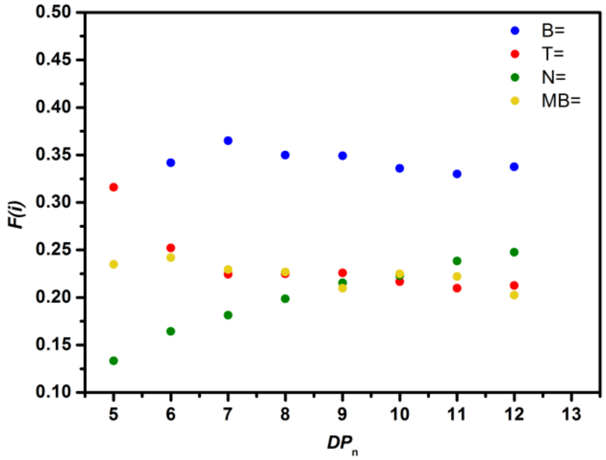

Figure S1. A plot of the mole fractions *F(i)* versus the degree of polymerization DP_n for all fragments of the three compared initiators (MMMP, Bz, 4MB) is shown.

Equations for ESI-MS Data Evaluation

(S1)
$$F^{X_1=}(i) = \frac{\Delta h^{DX_1=}(i)}{\Delta h^{DX_1=}(i) + \Delta h^{DX_2=}(i) + \Delta h^{DX_3=}(i)}$$

(S2)
$$G^{X=}(i) = \frac{\Delta h^{DX_1=}(i)}{\Delta h^{DX_2=}(i)}$$

(S3)
$$G'^{X=}(i, i-1) = \frac{\Delta h^{DX_1=}(i)}{\Delta h^{DX_2=}(i-1)}$$

(S4)
$$G''^{X=}(i, i+1) = \frac{\Delta h^{DX_1=}(i)}{\Delta h^{DX_2=}(i+1)}$$

(S5)
$$G^{X=}{}_{m/z,0} = \frac{G^{X=}(i) + G'^{X=}(i, i-1) + G''^{X=}(i, i+1)}{3}$$

Ionization and Solubility Effects in MMMP-initiated Polymer.

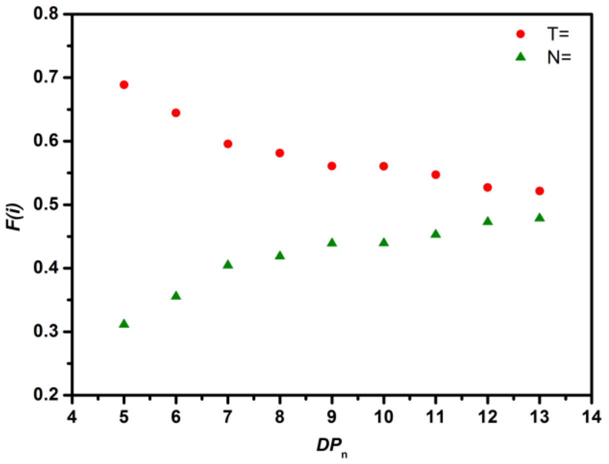

Figure S2. Plot of the mole fractions *F(i)* versus the degree of polymerization *DP*$_\mathrm{n}$ for the disproportionation peaks T= and N= for MMMP-initiated polymerization of EMA is shown.

Quantum Chemical Calculations

Photoinitiator	Singlet State	E_{rel} [eV]	Oscillator Strength [10^{-2}]	Triplet State	E_{rel} [eV]
Bz	S_1	3.406	0.661	T_1	2.968
	S_2	4.200	3.301	T_2	3.168
	S_3	4.267	0.074	T_3	3.589
	S_4	4.444	1.832	T_4	3.734
	S_5	4.848	25.004	T_5	4.096
4MB	S_1	3.440	0.673	T_1	2.996
	S_2	4.244	6.041	T_2	3.078
	S_3	4.324	0.116	T_3	3.592
	S_4	4.451	1.868	T_4	3.792
	S_5	4.676	29.952	T_5	4.149
MMMP	S_1	3.142	3.109	T_1	2.729
	S_2	3.984	33.907	T_2	2.874
	S_3	4.232	5.745	T_3	3.823
	S_4	4.360	0.046	T_4	3.941
	S_5	4.447	1.713	T_5	4.161

Table S1. Table view of selected singlet excitations and corresponding oscillator strengths as well as triplet excitations relative to S_0 calculated by TD-DFT/ B3LYP/aug-cc-pVDZ.

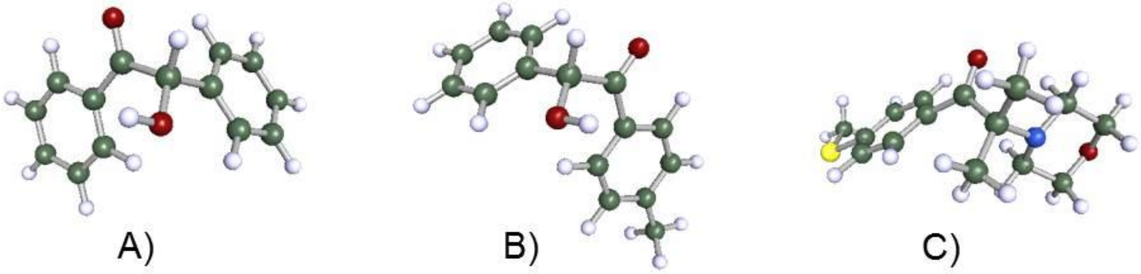

Figure S3. Optimized geometries of the trans structures of Bz, **A)**, and 4MB, **B)**. Based on their similar molecular structure, we found analog optimized minimum geometries for both Bz and 4MB characterized by a trans position of the hydroxyl and carbonyl group in good agreement with the literature.[1] **C)** shows the geometry-optimized structure of MMMP. As a result of the absence of a hydroxyl group and an asymmetric carbon atom neither cis nor trans positions can be distinguished.

	Bz	**4MB**	**MMMP**
S_0 [Hartree]	-690.82446	-730.11654	-1187.15327
$S_{0+\mathrm{corr.}}$ [Hartree]	-690.60335	-729.86837	-1186.81906

Table S2. Ground state energies without (S_0) and with ($S_{0+\mathrm{corr}}$) zero point correction at the minimum geometries. Compared to our previous findings[2] we found an energetically more stable structure of Bz of $1.46 \cdot 10^{-3}$ Hartree (< 0.0002 %). Thereby, the calculated geometries of Bz differ solely by the orientation of the hydrogen atom of the hydroxyl group causing a weak variation of the calculated energies.

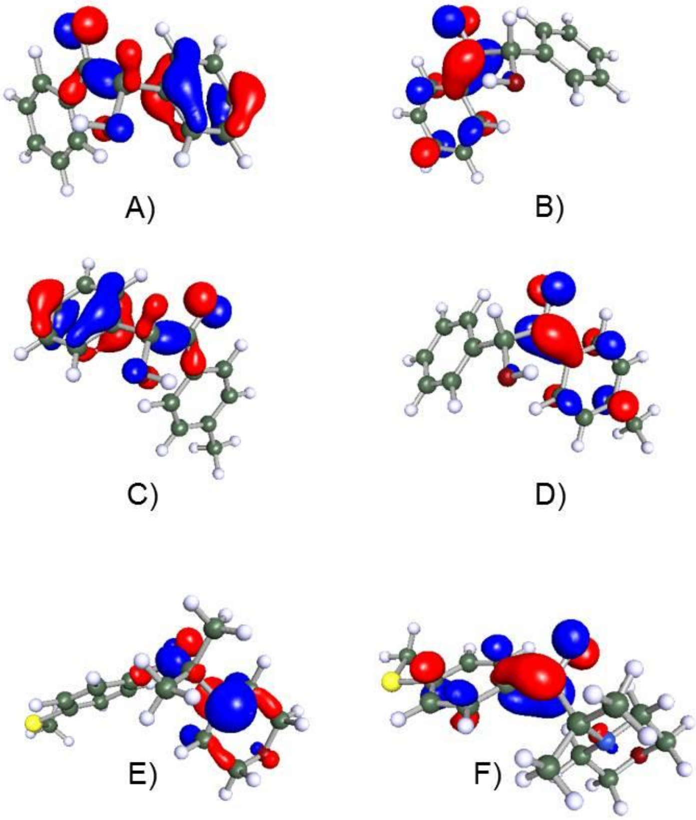

Figure S4. A)–B) HOMO and LUMO of Bz, **C)–D)** HOMO and LUMO of 4MB, and **E)–F)** HOMO and LUMO of MMMP. For Bz, the HOMO exhibits a lone pair character at the carbonyl oxygen combined with a slight π character on the phenyl ring, whereas the main contribution of the LUMO is described by π^*-character at the benzoyl ring and the carbonyl oxygen. The results for Bz are in good agreement with the literature[1] and can be sufficiently extrapolated to 4MB due to the similar molecular structure of the two molecules. The involved orbitals of the LUMO ← HOMO transition in MMMP are shown (**E)** HOMO and **F)** LUMO) and are in good agreement with a previous study.[3] Here, the contributions to the HOMO can be described by a lone-pair character of the carbonyl oxygen as well as, as a consequence of the absence of a phenyl ring, by a lone pair character of the nitrogen of the morpholino group. Furthermore, the

LUMO is specified by π* contribution of the benzoyl ring delocalized over the carbonyl oxygen, in agreement with Bz and 4MB.

Evaluation of Transient Data

351 nm / 477 nm	$A_{1,rel}$	$A_{2,rel}$	$A_{3,rel}$
Bz	0.59	0.35	0.06
4MB	0.49	0.29	0.22
351 nm / 501 nm			
Bz	0.62	0.37	0.01
4MB	0.51	0.28	0.21

Table S3. Relative amplitudes at a pump wavelength of 351 nm and probing at 477 nm and 501 nm for Bz and 4MB.

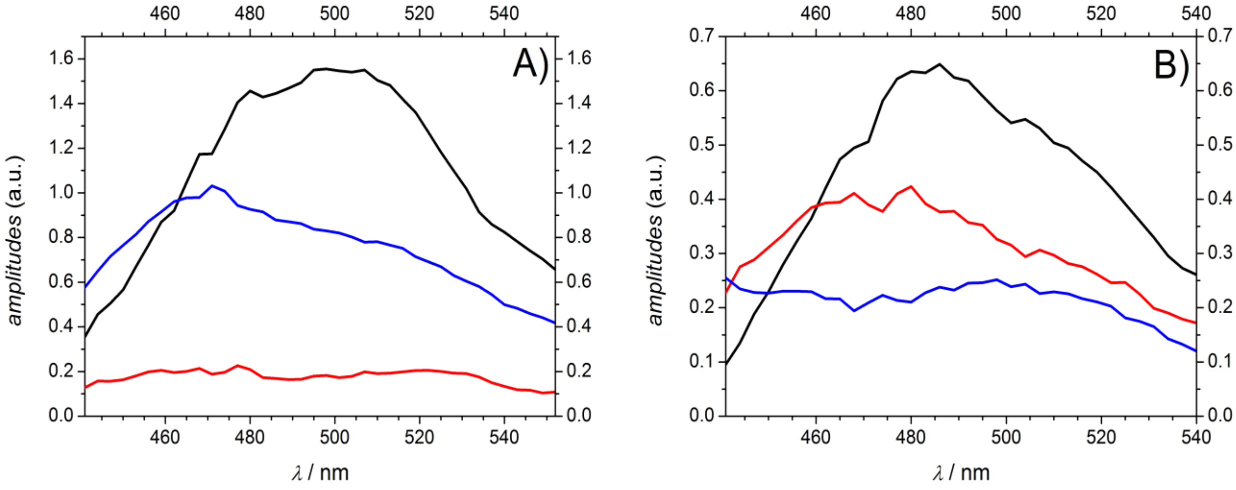

Figure S5. Amplitudes A_1 (black), A_2 (blue), and A_3 (red) derived from global fits for Bz (**A)**) and 4MB (**B)**) at a pump wavelength of 325 nm.

325 nm / 477 nm	$A_{1,rel}$	$A_{2,rel}$	$A_{3,rel}$
Bz	0.54	0.37	0.09
4MB	0.50	0.33	0.17
325 nm / 489 nm			
Bz	0.58	0.35	0.07
4MB	0.50	0.30	0.20
325 nm / 501 nm			
Bz	0.61	0.32	0.07
4MB	0.49	0.29	0.22

Table S4. Relative amplitudes at a pump wavelength of 325 nm and probing at 477 nm, 489 nm and 501 nm for Bz and 4MB. The first component shows the highest contribution to the TA for both initiators. Comparing the second and third components, $A_{3,rel}$ plays only a minor role for Bz, whereas these two components contribute nearly equally for 4MB.

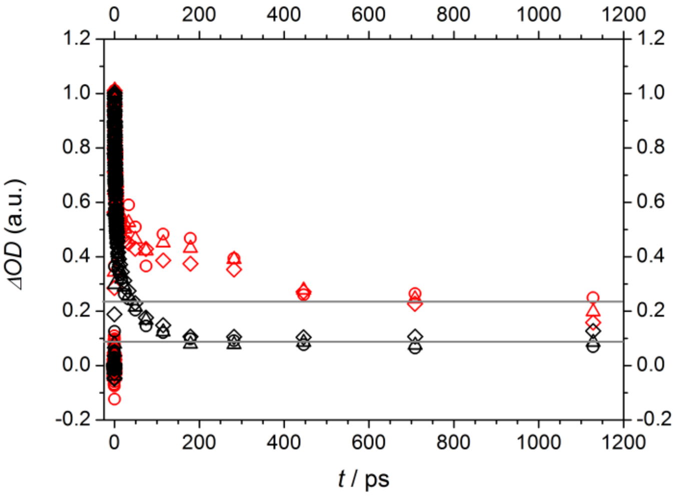

Figure S6. Normalized TA traces at three selected probe wavelengths 477 nm (square), 489 nm (triangle), and 501 nm (circle) at a pump wavelength of 325 nm for Bz (black) and 4MB (red). The relation between 4MB and Bz is determined by a factor of approximately 2.5 (grey lines: *ΔOD* (a.u.) = 0.09 for Bz and *ΔOD* (a.u.) = 0.23 for 4MB) indicating that 4MB shows a higher ability of radical formation.

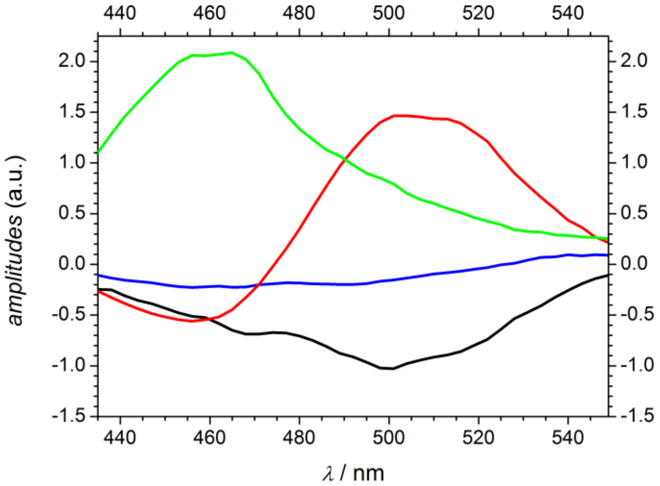

Figure S7. Amplitudes of MMMP derived from global analysis at a pump wavelength of 325 nm (A_1 black, A_2 blue, A_3 red, and A_4 green). The decay of the absorption band around 500 nm is directly connected to the development of the second absorption band (464 nm), which is apparent by positive and negative signature of A_3.

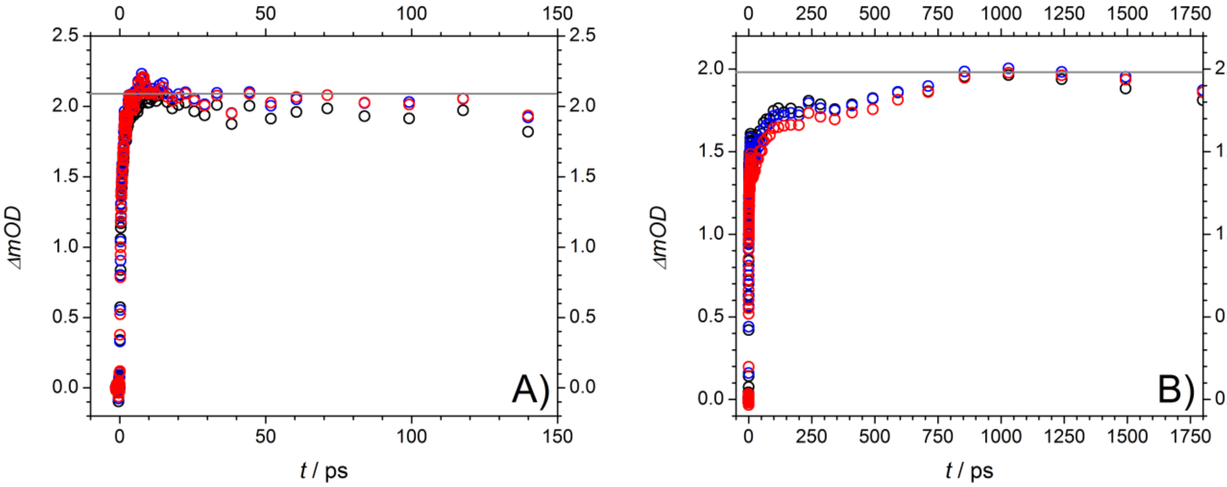

Figure S8. A) Singlet absorption band at 504 nm (black), 501 nm (blue), and 498 nm (red) (at a pump wavelength of 325 nm). **B)** Triplet absorption band at 468 nm (black), 465 nm (blue), and 462 nm (red) (at a pump wavelength of 325 nm). Assuming comparable absorption properties of both excited species the obtained TA values of 2.09 and 1.98 (grey lines), respectively, are a measure of the number of generated molecules in these two states and therefore for ISC efficiency origination from S_1. The relation between the obtained values is approximately 0.95 indicating a high population of T_1 (95 %).

REFERENCES

1. Z. Pawelka, E. S. Kryachko and T. Zeegers-Huyskens, *Chem. Phys.*, 2003, 287, 143-153.
2. T. J. A. Wolf, D. Voll, C. Barner-Kowollik and A.-N. Unterreiner, *Macromolecules*, 2012, 45, 2257-2266.
3. F. Morlet-Savary, X. Allonas, C. Dietlin, J. P. Malval and J. P. Fouassier, *J. Photochem. Photobiol., A*, 2008, 197, 342-350.